Desalination and Water Treatment
www.deswater.com
doi: 10.1080/19443994.2014.1002430

57 (2016) 5065–5078
March

Taylor & Francis
Taylor & Francis Group

Comprehensive study on the removal of chromate from aqueous solution by synthesized kaolin supported nanoscale zero-valent iron

Chuan Wang[a,1], Zhen Xu[a,b,1], Gang Ding[a], Xianxiang Wang[a], Maojun Zhao[a], Steven Sai Hang Ho[c], Yunchun Li[a,*]

[a]*College of Science, Sichuan Agricultural University, Ya'an 625014, P.R. China, Tel. +86 18283581575; email: 18283581575@163.com (C. Wang), Tel. +86 18257185100; email: 1334787373@qq.com (Z. Xu), Tel. +86 13982047472; email: 917492197@qq.com (G. Ding), Tel. +86 835 2886179; emails: xianxiangwang@hotmail.com (X. Wang), zmjun01@yahoo.com.cn (M. Zhao), Tel. +86 835 2886179; Fax: +86 835 2886136; email: yunchunli@sicau.edu.cn (Y. Li)*
[b]*Department of Chemistry, Zhejiang University, Hangzhou 310027, P.R. China*
[c]*Key Lab of Aerosol Science & Technology, SKLLQG, Institute of Earth Environment, Chinese Academy of Sciences, Xi'an 710061, P.R. China, Tel. +86 13609616516; email: steenho@hkpsrl.org*

Received 7 April 2014; Accepted 18 December 2014

ABSTRACT

A removal mechanism of chromate (Cr) by synthesized kaolin supported nanoscale zero-valent iron (K-nZVI) from aqueous solution is demonstrated. Parameters which potentially influenced the functioning of K-nZVI have been investigated as well. Based on the scanning electron microscopy, Fourier transform infrared spectroscopes, X-ray crystal powder diffraction and X-ray photoelectron spectroscopy identifications, we confirm that amorphous Fe^0 core/Fe_xO_y shell nZVI can be successfully loaded into the pores and cracks, and onto the surface of kaolin. Removal efficiency of Cr by K-nZVI decreased with increasing initial pH and Cr(VI) concentration, but increased while K-nZVI dosage increased. Humic acid and phosphate had similar dual impacts on chromium removal by K-nZVI, and the inhibitory effect was obvious at high concentrations in spite of their different reaction mechanisms. In contrast, high concentrations of sulfate and nitrate could advance the chromium removal. Adsorption isotherms indicate that the removal processes are endothermic. The data obtained can be better explained with Langmuir than Freundlich model. At the conditions of 318 K and optimized pH 4.0, the maximum adsorption capacity was 33.39 mg g^{-1} illustrating that K-nZVI was effective for the removal of total Cr. The removal mechanism is proposed to divide into four phases, including: (1) aqueous Cr(VI) ions are captured on the surface of K-nZVI; (2) the captured Cr(VI) are partly reduced to Cr(III) accompanied by Fe^0 oxidizing to Fe^{2+}; (3) part of oxidized Fe^{2+} continues to reduce Cr(VI); and (4) produced Cr(III), Fe^{2+}, and Fe^{3+} are formed passivation layers on the K-nZVI surface which prevent further removal of chromium and result in redundant Fe^0.

Keywords: Chromate; Kaolin; Supported nanoscale zero-valent iron; Removal mechanism

*Corresponding author.
[1]Chuan Wang and Zhen Xu contributed equally to this work.

1. Introduction

Chromium (Cr) is widely used in various industrial processes including metal plating, metal corrosion inhibition, pigment production, wood preserving, leather tanning, and petroleum refining. Anthropogenic activities such as accidental leakage and improper disposal can cause severe contaminations to fresh water resources and soils [1,2]. Even though chromium element manifests its necessity in vital movement, it leads to heavily toxic effects on organisms at relatively high concentrations [3]. In aquatic environment, chromium mainly exists in two oxidation states, trivalent chromium [Cr(III)] and hexavalent chromium [Cr(VI)], respectively; and the latter is known to be more toxic, mobile, and carcinogenic [4,5]. However, high concentration of Cr(III) beneficially inhibits various enzymatic activities due to its large capability coordinating with organic compounds [6]. Both inorganic and organic ligands in the environment can increase the solubility of Cr(III) through forming complexes [7]. Furthermore, the soluble complexes of Cr(III) can be re-oxidized to Cr(VI) either by naturally occurring oxidants or by chlorine-containing and other strong oxidizing disinfectants in drinking water treatment processing [7]. The United States Environmental Protection Agency (US EPA) has set a maximum contamination level of 0.1 mg L^{-1} for total chromium in drinking water [8,9]. It is thus vital to acquire an efficient chromium treatment or remediation technology.

Many studies have indicated that nanoscale zero-valent iron (nZVI), acting as a reducing agent, can effectively remediate a wide variety of environmental contaminants including chlorinated organic compounds, heavy metal ions, inorganic anions, and radionuclides [10]. nZVI is widely used for *in situ* remediation due to its higher degradation rates for contaminants and larger capacity for injection into the subsurface compared with other bulk materials. However, there are still technical challenges associated with its application. Both rapid aggregations of bare nZVI related to its intrinsic magnetic attraction and attachment to sand grains can limit the transportability in porous media [10]. In addition to the intrinsic properties of nZVI, many environmental factors can also affect its stability, deliverability, targeting ability, and reactivity during *in situ* remediation [11]. As a result, modification of nZVI must be required to overcome the current weaknesses. Polymeric surface modification, emulsification, and embedding or supporting nZVI to a carrier are three major modified alternatives. Among them, nZVI embedded in carriers or supports are widely applied because both physical adsorption and chemical reduction contribute to the remediation. Polyflon resin-supported nZVI particles were used to remediate Cr(VI) and Pb(II) from aqueous solutions. Its rate of remediation for Cr(VI) and Pb(II) was up to 30 times higher than that offered from iron filing or iron powder on a Fe molar basis [12]. Chitosan-stabilized nZVI particles were found to have increased stability as nitrogen and oxygen atoms on the chitosan bound to iron. Experiments also demonstrated that the maximum Cr(VI) reduction rates by chitosan-stabilized nZVI was about three times higher than that using nZVI alone [13]. Besides, bentonite-, pillared bentonite-, black carbon-, natural montmorillonite-, and HDTMA modified montmorillonite-supported nZVI have been showed better removal efficiencies compared to unsupported nZVI [11,14–17].

Only limited studies have investigated the Cr(VI) removal mechanism and the influence of natural occurring ligands [such as phosphate, sulfate, nitrate, and humic acid (HA)] on the transformation of chromate by nZVI or supported nZVI. In addition, with respect to support substance, kaolin, acting as one major kind of clay minerals, manifests a variety of advantages including chemical and mechanical stability, high specific surface area, bargain price, and natural abundance. To our best knowledge, studies on kaolin adsorbing of heavy metal cations such as Pb(II), Cd(II), Ni(II), Cu(II), and Co(II) [18,19] were being drawn more attention accounting for high cation exchange capacity or strong cationic surface complexation capacity as well as electrostatic attraction. In contrast, the removal of heavy metal anions (e.g. arsenate and dichromate) by kaolin was rarely reported.

The aim of this study is to investigate physicochemical factors affecting chromate removal by synthesized kaolin supported nanoscale zero-valent iron (K-nZVI) from aqueous solution and its operating mechanism. Details of preparation steps for K-nZVI with liquid phase chemical reduction have been shown. In addition, potential influences on the chromate removal efficiency, including pH, K-nZVI dosage, initial Cr(VI) concentration and presence of co-existing ions (phosphate, sulfate, and nitrate), and HA have been investigated and demonstrated. The maximum adsorption capacity was studied through adsorption isotherms. Furthermore, the removal mechanism of chromate by K-nZVI has been explored through scanning electron microscopy (SEM), Fourier transform infrared spectroscopes (FTIR), X-ray crystal powder diffraction (XRD), and X-ray photoelectron spectroscopy (XPS) characterizations.

2. Materials and methods

2.1. Materials and reagents

Kaolin, provided by Fengxian Fengcheng Reagent Factory (Shanghai, China), was in chemical purity. The solutions of phosphate, sulfate, nitrate, calcium, sodium, and magnesium were prepared from bulks of NaH_2PO_4, K_2SO_4, KNO_3, $CaCl_2$, NaCl, and $MgCl_2$, respectively. Except KBr was in spectral purity, all of the reagents were analytical grade. Distilled water was used to prepare the aqueous solution. The standard solutions of iron and chromium (1,000 mg L^{-1}, NACIS, China) were used in atomic absorption spectrophotometry (AAS-6300, Shimadu, Japan).

2.2. Synthesis of K-nZVI and nZVI

K-nZVI was prepared by the liquid phase chemical reduction method as involved in pertinent literatures [18,20]. Briefly, 0.1 mol L^{-1} ferrous solution was prepared by dissolving 1.389 g of $FeSO_4{\cdot}7H_2O$ in 50 mL mixed liquor of absolute ethanol and water (2:3 v/v), which was transferred into a three-necked flask containing kaolin, and then deaerated under the flow of ultrapure nitrogen (N_2) with magnetic stirring for 30 min. Afterwards, 100 mL of 0.15 mol L^{-1} $NaBH_4$ solution, employed as reductant, was dropwisely instilled into the mixture by a tap funnel and additionally stirred for 20 min. To guarantee the complete reduction of Fe^{2+}, six times of stoichiometric dosage of $NaBH_4$ was used. The entire process was simultaneously stirred under N_2 atmosphere. The generated black substances were filtrated in vacuum and rinsed for three times with distilled water, absolute ethanol and acetone, respectively. To prevent the oxidation of synthesized nZVI, the black substances were forbidden to explore into air through the rinsing steps. Finally, the black material was dried immediately in the chamber of an EYELA FDU-2200 freeze-dryer (Tokyo Rikakikai, Tokyo, Japan) overnight and then preserved under N_2 atmosphere in a desiccator. K-nZVI with various Fe mass contents (wt.%) was prepared as the above-mentioned procedures with a range of kaolin loadings. nZVI was prepared without kaolin. Actual iron contents were measured by AAS through dissolving 0.05 g of K-nZVI with appropriate amount of HNO_3 and HCl. The comparison results are given in Table 1. The actual iron contents in K-nZVI were slightly lower than the theoretical values, indicating that synthesized nZVI was not fully supported onto kaolin and then filtrated. It has been reported that the removal efficiency of Pb(II) by K-nZVI increased with an increasing contents of nZVI, but remained constant at a level between 20 and 25% [18]. In order to remove cost-effectively, K-nZVI containing 20% nZVI was thus applied in all the following experiments.

Table 1
Comparison between theoretical and actual iron contents in K-nZVI

Weight of $FeSO_4{\cdot}7H_2O$/g	Weight of kaolin/g	Iron content (wt.%)	
		Theoretical	Actual
1.389	5.301	5.0	3.8
	2.511	10.0	7.3
	1.116	20.0	16.5
	0.651	30.0	25.7
	0	nZVI	

2.3. Characterizations and measurements

SEM images of K-nZVI were obtained using a JSM-7500F SEM (JEOL, Japan) at an operating voltage of 50 kV. The specific surface areas of nZVI, K-nZVI, and kaolin were determined by Brunauer–Emmett–Teller (BET) adsorption method. The FTIR spectra of K-nZVI were observed via a FTIR spectrometer (Shimadzu FTIR-8400S, Japan) ranging of 4,000–400 cm^{-1} with a resolution of 4 cm^{-1}. XRD measurements of nZVI, kaolin, and K-nZVI were performed on an UltimaIV diffractometer (Rigaku Corporation, Japan) using Cu Kα radiation ($\lambda = 0.154056$ nm) at a scan rate of 15° min^{-1}. The tube source was operated at 40 kV and 30 mA. XPS data of K-nZVI were acquired using a Kratos XSAM800 with an Al Kα monochromatic source radiation (225 W). XPS measurements were operated in the constant pass energy mode with full spectrum measurement at 160 eV and high resolution spectra at 40 eV for Cr 2p, Fe 2p, and C1s.

2.4. Batch experiments

A stock solution of 1,000 mg L^{-1} Cr(VI) was obtained by dissolving K_2CrO_4 into distilled water. Working solutions of Cr(VI) were prepared from the stock solution by dilution. In the batch experiments, 0.1 g K-nZVI and 50 mL, 50 mg L^{-1} Cr(VI) solution (fixed initial pH 4.0) were mixed well in conical flask and placed on a thermostatic shaker bath at 25°C, and then stirred with 160 rpm for 12 h. The supernatant was collected after centrifugation with a speed of 4,000 rpm for 10 min. The total Cr concentration was analyzed with AAS. The removal efficiency of total Cr (R (%)) was calculated by the equation: R (%) = $(C_0 - C_t)\ 100/C_0$, where C_0 (mg L^{-1}) is the initial Cr (VI) concentration and C_t (mg L^{-1}) is the total concen-

tration of Cr in solution at time t. All experiments were conducted in duplicate. All points in the figures were shown by the mean values and error bars represented their standard deviation. All standard deviations (<3%) are in line with the requirements.

The effects of several parameters were investigated. For each, only one parameter varied while the others remained constant as above-mentioned condition, except the study of K-nZVI dose with 100 mg L^{-1} of initial Cr(VI) concentration. Initial pH (3–10) was adjusted using 0.1 M HCI or NaOH. Different initial Cr(VI) concentrations in a range of 10 and 80 mg L^{-1} were performed. The effect of K-nZVI dose was set between 0.01 and 0.30 g. For comparison in the dosage experiment, 0.1 g kaolin and 0.1 g nZVI instead of K-nZVI was added into 50 mL of 100 mg L^{-1} Cr(VI), respectively. The effects of common anions (phosphate, sulfate, and nitrate), cations (calcium, sodium, and magnesium), and HA on the removal of Cr(VI) by K-nZVI were investigated. Sulfate, nitrate, and HA were applied at the concentrations ranged from 0.5 to 100 mg L^{-1}, while phosphate at the concentrations ranged from 0.5 to 50 mg L^{-1}. All of cations were studied in a range of 0.5 and 30 mg L^{-1}. Individual co-existing ion was added into a mixture of 50 mL of 50 mg L^{-1} Cr(VI) solution (pH 4.0) and 0.1 g K-nZVI. In addition, the control experiment was conducted without adding any co-existing ions or HA.

2.5. Adsorption isotherms

The adsorption isotherm experiments were carried out by adding 0.1 g synthesized K-nZVI to 50 mL of initial Cr(VI) concentrations (C_0 (mg L^{-1})) ranged from 10 to 80 mg L^{-1} (pH 4.0) at different temperatures (298, 308, and 318 K, respectively). The following processes were as same as that shown in batch experiments. The equilibrium adsorbed amount of Cr (q_e (mg g^{-1})) was evaluated according to the equation: $q_e = (C_0 - C_e)V/m$, where V and m are the total volume of the solution (L) and the adsorbent mass (g), respectively. C_e (mg L^{-1}) is the equilibrium concentration of total Cr in solution. The adsorption isotherms were fitted by the Langmuir and Freundlich models.

3. Results and discussion

3.1. Characterizations

3.1.1. SEM analysis

The morphologies of K-nZVI before and after reaction with Cr(VI) are illustrated in Fig. 1. The SEM images before reaction (Fig. 1(a) and (b)) show that the majority of the synthesized nZVI supported on kaolin were spherical shaped nanoparticles (<100 nm in diameter) and loaded into the pores or cracks and onto the surface of kaolin. It can be seen that nZVI exhibited good dispersion with little aggregation on the kaolin. However, after reaction, the dimension of iron nanoparticles increased distinctively and the surface of K-nZVI seemly coated by products, which resulted in the disappearance of mainly pores or cracks of K-nZVI (Fig. 1(c) and (d)). This implies that Fe^0 corrosion and co-precipitation were involved. It also supports evidence for the hypothesis that both adsorption, redox reaction and precipitation took place in the removal of Cr(VI) by K-nZVI [11,20].

3.1.2. FTIR spectrogram

The FTIR spectra of K-nZVI before and after removal of Cr(VI) are shown in Fig. 2. The sharp peaks at 3,694 and 3,620 cm^{-1} corresponding to OH-stretching imply a high H_2O molecule content in the kaolin mesosphere and octahedron before reaction, as well as obvious kaolin peaks of OH-bending at 1,104, 1,033, 1,010, 914, 792, 754, and 695 cm^{-1} (Fig. 2(a)) [21,22]. However, the characteristic peak was shifted from 1,104 to 1,106 cm^{-1} and the peaks located at 1,033 and 1,010 cm^{-1} were transformed into a broad absorption band after reaction (Fig. 2(b)), suggesting that partial Al–O–H bonds was destructed during removal process. Consistent well with the nZVI spectra bands reported by Zhang et al. [21], the absorption peaks at 470 and 540 cm^{-1} characterizing Fe–O stretch of Fe_2O_3 and Fe_3O_4, respectively, were observed before and after reaction, confirming that nZVI had been successfully supported on kaolin and its surface was partially oxidized. This supports the hypothesis that K-nZVI had the Fe^0 core/Fe_xO_y shell structure [21].

3.1.3. XRD measurements

Fig. 3 shows XRD patterns of nZVI, natural kaolin, synthesized K-nZVI before and after reaction. The interpretation of the XRD spectra allows us to analyze the phase composition of material. Synthesized nZVI particles can be characterized by the sharp peak at ~44.7° (Fig. 3(a)), suggesting that there is large crystalline grain size and high crystallinity. Meanwhile, the ignorable intensity of iron oxide (Fe_xO_y) diffraction peaks (at 30° and ~35°) [21,23,24] elucidates that the content of oxide kept at a relatively low level. Peak M (Fig. 3(c)) is in good accordance with (1 1 0) crystal face in Fig. 3(a). Thus, as expected, nZVI was successfully

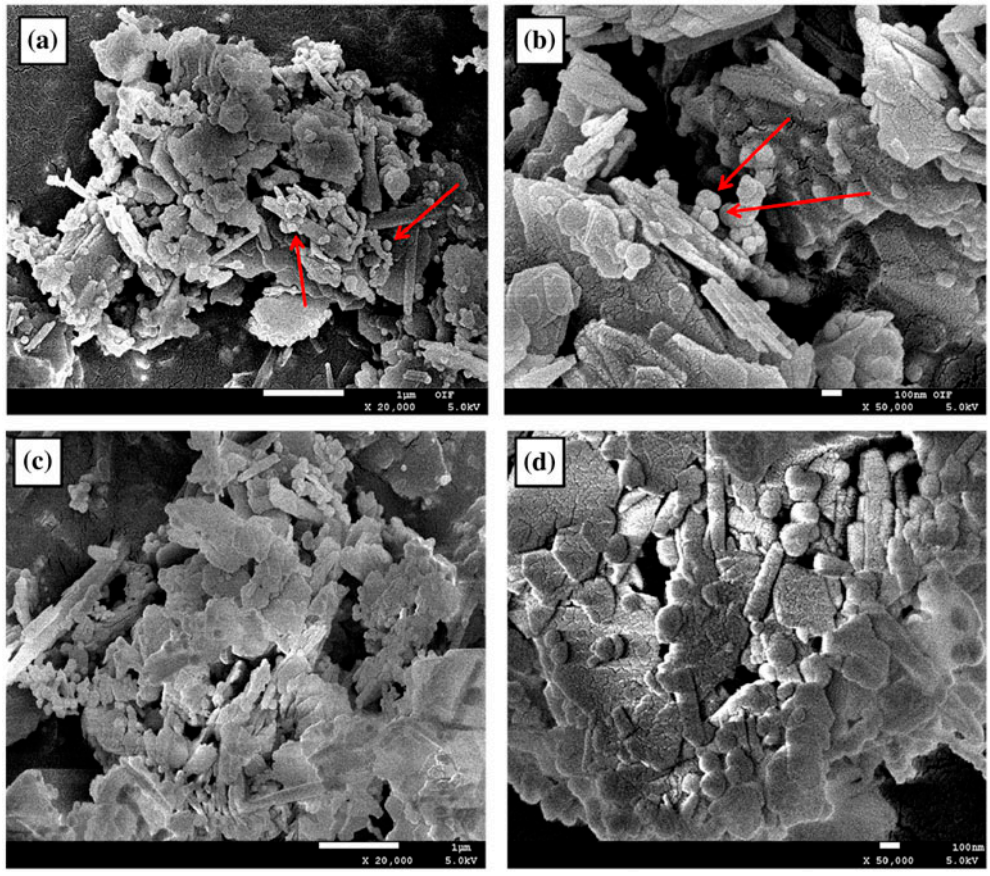

Fig. 1. SEM images of K-nZVI before and after reaction with Cr(VI): (a) before reaction (×20,000), (b) before reaction (×50,000), the red arrows point to the spherical-shaped nanoparticles, (c) after reaction (×20,000), and (d) after reaction (×50,000).

loaded on kaolin substrate. Compared with the corresponding peak L and M in Fig. 3(b) and (c), respectively, even though they are partially overlapped, peak M is more broaden and higher relative intensity than peak L. The possible reasons are the generation of amorphous phase of iron [24] and smaller crystalline grain size after loaded on kaolin (carrier contributes to reducing the specific surface energy of nZVI).

3.2. Batch experiments

3.2.1. Effect of initial pH

Fig. 4 illustrates that the initial pH value plays an important role in the removal of Cr(VI) by K-nZVI. With the initial pH increased from 3.0 to 10.0, the removal efficiency dropped significantly from 99.73% to 49.36%. The result also indicates that the total Cr removal has maximum efficiencies (in a range of 99.46% and 99.73%) at a low pH values (from 3.0 to 5.0). As a result, pH 4.0 is defined as its optimum operation value. In general, Cr(VI) exists different

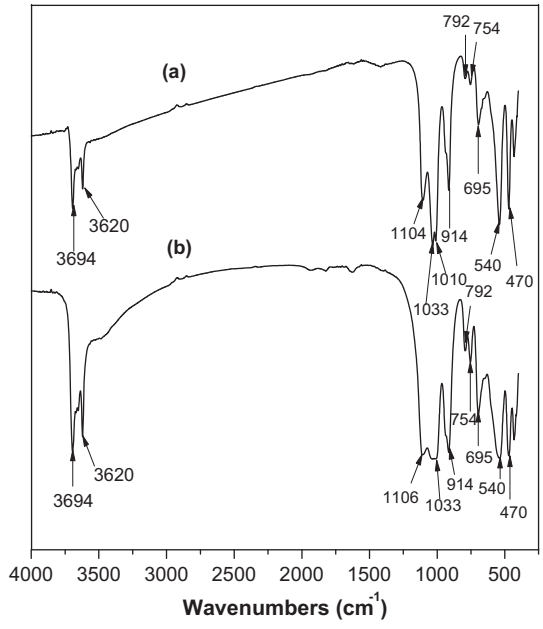

Fig. 2. FTIR spectra of K-nZVI before (a) and after (b) reaction with 50 mg L^{-1} of Cr(VI) solution.

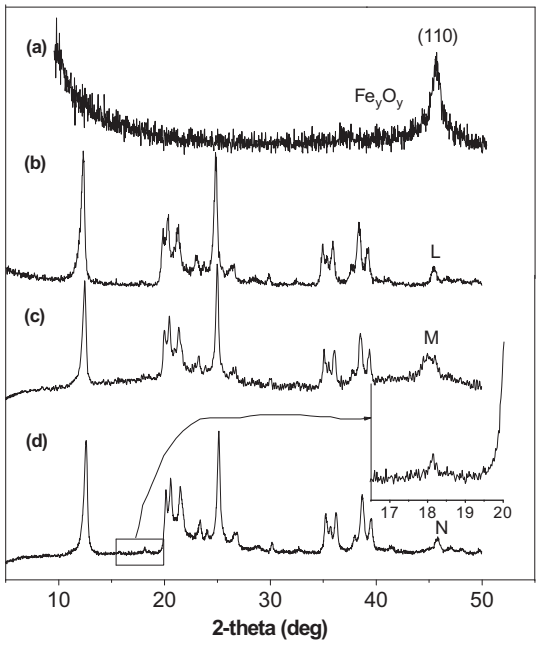

Fig. 3. XRD patterns of samples. (a) nZVI, (b) kaolin, (c) K-nZVI before reaction, and (d) K-nZVI after reaction with 50 mg L^{-1} Cr(VI) solution (the insert represents microscope of two-theta in the range of 16.5°–20°).

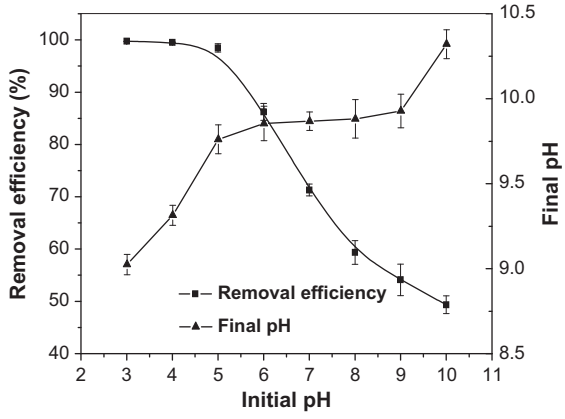

Fig. 4. Effect of initial pH on the removal of total Cr by K-nZVI (reaction between 50 mg L^{-1} Cr(VI) and 0.1 g K-nZVI at 25°C, 160 rpm for 12 h).

ionic forms in aqueous solutions under variable pH values [4,25]. The dominant species of Cr(VI) is $HCrO_4^-$ at pH < 6.1, and gradually transforms into CrO_4^{2-} with the increased pH [26]. However, $HCrO_4^-$ is easier to be adsorbed than CrO_4^{2-} because of its lower adsorption free energy [26]. In addition, pH can create a contribution to the surface charge of K-nZVI. Adsorbent is negatively charged when pH is above the point of zero charge, which leads more electrostatic repulsion between Cr(VI) ions and K-nZVI, and consequently causes the decrease of removal efficiency. Our result is consistent with other findings that the Cr(VI) removal efficiency by activated carbon-based iron-containing adsorbents and nZVI-Fe_3O_4 nanocomposites declined sharply <20% and <40% while the pH increased to 11 and 10, respectively [9,26].

As removal mechanism to be described next, Cr(VI) is partly reduced to Cr(III) by Fe^0 or Fe^{2+}. Subsequently, almost all Cr(III) is removed in the form of hydroxylated and co-precipitations (e.g. $Cr(OH)_3$, $Cr_xFe_{1-x}(OH)_3$, or $Cr_xFe_{1-x}OOH$ [8]) that obstructs the electron transfer and abrogates further reactions. However, the formations of these precipitations are inhibited at acidic environments according to Eqs. (1) and (2) [8]. At lower pH values, Cr(VI)/Cr(III) possesses higher positive electrode potential (Eqs. (3) and (4)) which leads to more significant reduction of Cr(VI) by Fe^0. Xie and Cwiertny [27] proposed that more quantities of ferrous iron species, which are the dominant substances for Cr(VI) removal by nZVI below pH 8, were produced because of higher corrosion rate at low pH values. Our results clearly show that final pH increased gradually and varied in a range of 9.02 and 10.32 after reaction while the initial pH increased. This implies that removal of Cr(VI) was the process of proton consumption and little Cr(III) was released into the solution due to low solubility product of $Cr(OH)_3$. Hence, the increasing pH results in negative removal efficiency and K-nZVI can effectively remediate Cr(VI) and Cr(III) at the lower pH level.

$$xCr^{3+} + (1-x)Fe^{3+} + 3H_2O = Cr_xFe_{1-x}(OH)_3(s) + 3H^+ \quad (1)$$

$$xCr^{3+} + (1-x)Fe^{3+} + 2H_2O = Cr_xFe_{1-x}OOH(s) + 3H^+ \quad (2)$$

$$HCrO_4^- + 7H^+ + 3e^- = Cr^{3+} + 4H_2O \quad (3)$$

$$CrO_4^{2-} + 8H^+ + 3e^- = Cr^{3+} + 4H_2O \quad (4)$$

3.2.2. Effect of initial Cr(VI) concentration

Fig. 5 illustrates the effect of initial Cr(VI) concentration (C_0) on its removal efficiency by K-nZVI. It can be seen that removal efficiency exceeded 99% with little variation in the range of 10 and 25 mg L^{-1}, but decreased to 92.3% as C_0 increased to 40 mg L^{-1}, and further dropped to 66.3–82.3% at $C_0 \geq 60$ mg L^{-1}. In

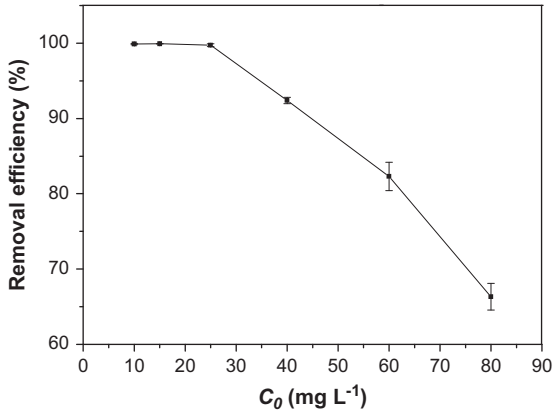

Fig. 5. Effect of initial Cr(VI) concentration on the removal of total Cr by K-nZVI (reaction with 0.1 g K-nZVI at pH 4.0, 25°C, 160 rpm for 12 h).

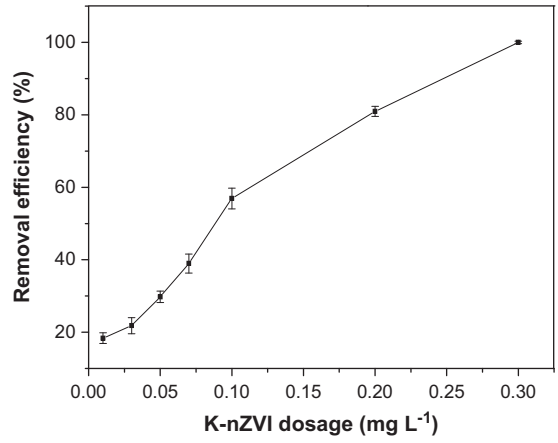

Fig. 6. Effect of K-nZVI dosage on the removal of total Cr by K-nZVI (reaction with 100 mg L^{-1} Cr(VI) at pH 4.0, 25°C, 160 rpm for 12 h).

prior investigation of Cr(VI) removal by chitosan-Fe^0, Geng et al. [28] assumed that reduction of Cr(VI) to Cr(III) occurred on the reactive sites occupied by Fe^0, while no reduction happened on the nonreactive sites occupied by other substances rather than Fe^0. Similarly, because of the existence of iron oxide impurities, we hypothesize that both reactive sites and nonreactive sites existed on the K-nZVI surface, and the reactive sites remained constant at a fixed amount of K-nZVI. Almost complete removal of total Cr at low C_0 range indicates that the reactive sites were not saturated. However, removal efficiency decreased while C_0 further increased, implying that the limited reactive sites were saturated and then acted as a hindrance for the lasting of reduction.

3.2.3. Effect of K-nZVI dosage

Fig. 6 shows the removal efficiency of Cr as a function of K-nZVI dosage. It is clear that the removal efficiency increased with the K-nZVI dosage aggrandizing. This observation can be ascribed to the increase of reactive sites as iron contents strengthened. However, removal efficiency below 0.1 g dosage presents a faster growth trend than that of above 0.1 g, and only 56.92% of Cr was removed at iron contents of ~3.3 times the stoichiometric quantity. The most possible reasons are the formation of passivation layer (as the following discussed in removal mechanism) and occurrence of side reactions with water and dissolved oxygen [12]. The higher dosage is, the more remarkable side reactions can be. In the control experiment, poor removal efficiency of kaolin (1.35%) might be due to no reduction and low adsorption capacity of kaolin for Cr(VI). Furthermore, it is found that the Cr removal efficiency by 0.1 g K-nZVI (56.92%) was much higher than the sum (30.8%) of the reduction by 0.1 g nZVI (29.45%) and the adsorption by kaolin (1.35%). This confirms that kaolin, as a supporter, not only stabilizes and disperses nZVI but also prevents its aggregation and provides more reactive sites based on the same Fe^0 mass. In addition, this phenomenon indicates that the Cr removal by K-nZVI is not a simple sum of adsorption and reduction. There must be some synergetic effect existing between kaolin and nZVI.

3.2.4. Effects of HA and co-existing ions

Natural groundwater usually consists of various cations, anions, and humic substances, mainly HA, which may influence the removal of chromium by K-nZVI. Therefore, in practical application, we need to take them into consideration. In present work, compared to HA and anions (nitrate, sulfate, and phosphate), cations (sodium, calcium, and magnesium) did not obviously change the removal efficiency (the results are not shown). The possible reasons are electrostatic repulsion between cations and K-nZVI, and cations could not form inner-sphere complexes.

Fig. 7 shows the effects of three anions and HA on the chromium removal. Compared to the control experiment (R = 89.1%), the low concentrations of HA (0.5–10 mg L^{-1}) improved the removal efficiency (R = 90.3–94.4%), while high concentrations of HA (10–100 mg L^{-1}) depressed the removal efficiency (R = 63.9–90.3%). In the natural environment, HA was considered as an important reducing agent [29]. So improved removal efficiency at low levels of HA might result from the reduction of Cr(VI) or Fe(III) by HA. In addition, the quinones in HA would play

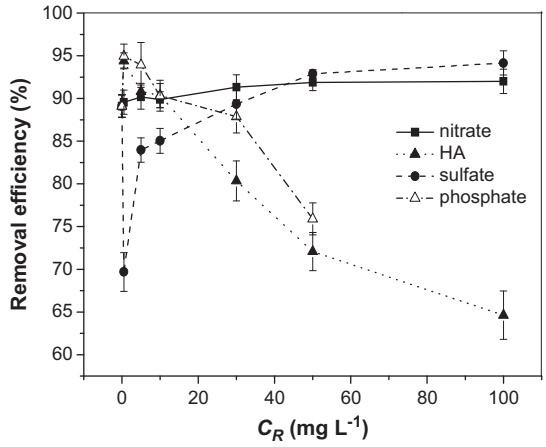

Fig. 7. Effects of co-existent anions and HA on the removal efficiency (C_R is the initial concentration of ions and HA; reaction between 50 mg L^{-1} Cr(VI) and 0.1 g K-nZVI at pH 4.0, 25℃, 160 rpm for 12 h).

the role of electron shuttles to strengthen electron transfer [30]. However, as content of HA was further raised, the side reaction between dissolved oxygen and K-nZVI might be enhanced and the formation of Fe(III)-humate complexes and Cr(III)-humate complexes were increased, which were further ascribed to dissolved chromium concentration [7]. As a result, HA possesses dual impacts on chromium removal by K-nZVI, that is, low concentrations of HA promoted chromium removal, while high concentrations of HA suppressed.

Similar to HA, phosphate had dual impacts on chromium removal by K-nZVI. In concentration ≤10 mg L^{-1} of phosphate enhanced the chromium removal (e.g. R = 94.9% at 0.5 mg L^{-1} phosphate), while higher than that had a negative influence to some extent (e.g. R = 75.9% at 50 mg L^{-1} phosphate). Phosphate exploiting oxygen atoms can form Fe-complexes with Fe(III) and Fe(II), and Fe(III)-complexes are more stable than Fe(II)-complexes [7], which resulted in the decrease of the electrode potentials of Fe(II)/Fe^0 and Fe(III)/Fe(II) and increased the removal efficiency. The transferring electrons from Fe^0 to Fe^{2+} or from Fe^{2+} to Fe^{3+} could either be gained by dissolved oxygen or Cr(VI) [27]. In this study, depressed removal efficiency in high levels of phosphate suggests that the electron transfer presented a preference for dissolved oxygen. Eary and Rai [31] proposed that the molar ratios of oxidized Fe(II) to reduced Cr(VI) were accelerated as the concentration of phosphate enhanced.

Contrary to HA and phosphate, sulfate depressed the removal efficiency in low concentrations while enhanced the removal efficiency in high concentrations. Specifically, removal efficiency fell markedly to 69.7% at 0.5 mg L^{-1} sulfate, and then gradually increased to 94.2% while sulfate increased to 100 mg L^{-1}. Such phenomenon indicates that low concentrations of sulfate apparently competed the reactive sites with Cr(VI). The improved removal efficiency at high levels of sulfate should be ascribed to the fact that sulfate could accelerate electron generation as a corrosion promoter [27], thus created more reactive sites on the iron surface. Iron corrosion and electron release were the prerequisites of pollutant degradation [32]. And it has been suggested that sulfate promotes the corrosion of Fe^0 through destabilizing the passivation layers on the iron surface [33].

However, compared to HA, phosphate, and sulfate, nitrate had slight acceleration on the chromium removal in the whole studied range (0.5–100 mg L^{-1}), because the external addition of nitrate reinforced the ionic strength and then encouraged iron corrosion [32]. At the concentration of 100 mg L^{-1} co-existing ions, nitrate had slightly lower removal efficiency (92.0%) than sulfate (94.2%). This difference was ascribed to stronger ion strength provided by sulfate than nitrate with the same concentration. Despite phosphate could contribute stronger ion strength and improve iron corrosion, the inhibitory effects from many aspects in high concentrations were more manifest. Nitrate seems not to form stable inner-sphere complexes with iron (oxy) hydroxides as phosphate does. Thus competitive capacity of nitrate for the reactive sites was not considered to be stronger than or as effective as chromate. Analogous phenomenon that nitrate could not compete reactive sites with bromate was observed by Xie and Shang [34]. Many studies have confirmed that nitrate could be reduced by Fe^0. However, this reaction was an acid-driven [32,35]. As mentioned previously, both H^+ consumed and OH^- released during chromate reduction by K-nZVI contributed to the pH increase, which inhibited the nitrate reduction by K-nZVI. Therefore, the reaction between nitrate and K-nZVI was negligible in current system. To summarize, a conceptual model was established to depict the effecting process of anions and HA (Fig. 8).

3.3. Adsorption isotherms

Temperature is another important parameter in K-nZVI treatment systems. It can be seen from Fig. 9 that the q_e increased with the raise of temperature indicating the endothermic nature of removal process. Similar phenomenon was also observed in the removal of crystal violet by K-nZVI [20]. In order to have better understanding of the removal mechanism, the experiments were carried out by applying two well known

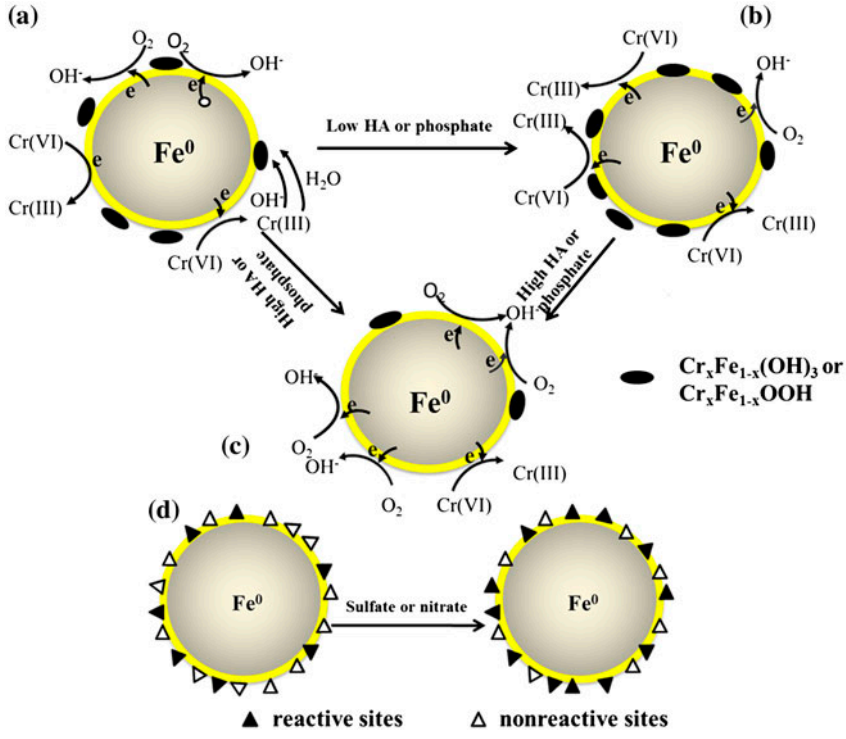

Fig. 8. Conceptual model of chromate removal by K-nZVI in the present of co-existing ions and HA: (a) without co-existing ions, Cr(VI) was reduced by K-nZVI, and then formed mixed Cr(III)/Fe(III) precipitates; (b) Cr(VI) reduction and precipitates were increased in the low HA or phosphate concentrations; (c) Cr(VI) reduction and precipitates were decreased in the high HA or phosphate concentrations; (d) more reactive sites on the K-nZVI surface were created in the present of sulfate or nitrate.

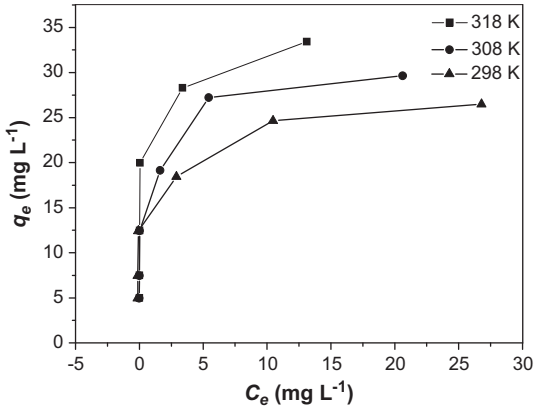

Fig. 9. Plots of the equilibrium absorbed amount versus the equilibrium concentration of total Cr at different temperatures (reaction with 0.1 g K-nZVI at pH 4.0, 160 rpm for 12 h).

isotherms, Langmuir and Freundlich, respectively [9]. The Langmuir model assumes that monolayer adsorption occurs to homogeneous surface with a limited number of adsorption sites, all of which are identical and energetically equivalent. The linear form of Langmuir equation was described as follows:

$$\frac{C_e}{q_e} = \frac{1}{q_m b} + \frac{C_e}{q_m} \tag{5}$$

where q_m (mg g^{-1}) is the maximum adsorption capacity and b is the Langmuir constant relating to the energy of apparent adsorption. The constants b and q_m listed in Table 2 are evaluated by the intercept and slope of plot of C_e/q_e versus C_e, respectively. The values of q_m and b increased with the raise of temperature implying that the adsorption capacity was higher and the energy of apparent adsorption was lower at higher temperatures. In this study, q_m (33.39 mg g^{-1}) of Cr removal by K-nZVI was 9.5 times that of bare nZVI at 318 K [36]. It is worth to note that the removal capacity of Cr by K-nZVI was much higher than naked nZVI as a result of the aggregation of nZVI decreasing for K-nZVI, despite nZVI had a larger specific surface area (104.38 m^2 g^{-1}) than K-nZVI (17.54 m^2 g^{-1}).

Table 2
Langmuir and Freundlich adsorption isotherm parameters for total Cr removal by K-nZVI

	Langmuir			Freundlich		
Temperature (K)	b	q_m	r^2	K_f	$1/n$	r^2
298	2.4035	26.67	0.9966	15.483	0.1849	0.8933
308	3.5207	29.93	0.9974	13.219	0.1715	0.9151
318	9.1868	33.39	0.9972	24.459	0.1298	0.8666

For the Langmuir isotherm, a dimensionless constant separation factor can be expressed by the following expression

$$R_L = \frac{1}{1 + bC_0} \tag{6}$$

The value of R_L indicates the type of isotherm to be either unfavorable ($R_L > 1$), linear ($R_L = 1$), favorable ($0 < R_L < 1$), or irreversible ($R_L = 0$). Fig. 10 shows that the values of R_L at different C_0 and temperatures fell into the range of 0–0.04 indicating that the removal process of Cr(VI) is favorable. Simultaneously, the values of R_L decreased markedly as C_0 and temperature increased, implying more favorable adsorption at higher concentrations and temperatures.

The Freundlich isotherm is derived from the hypothesis of physical adsorption on a heterogeneous adsorbent surface. The linear relationship of Freundlich equation is given as:

$$\log\ q_e = \log\ k_f + \frac{1}{n}\log\ C_e \tag{7}$$

where k_f and $1/n$ are the Freundlich constants related to the adsorbent capacity and intensity, respectively.

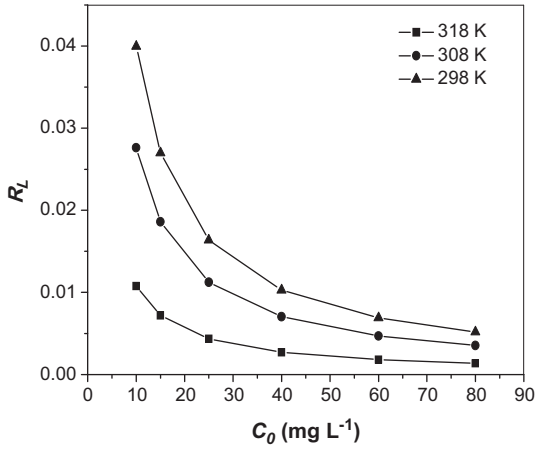

Fig. 10. Relationship between separation factor and initial Cr(VI) concentration at different temperatures.

The constants k_f and $1/n$ listed in Table 2 are evaluated by the intercepts and slopes of plots of log q_e versus log C_e, respectively. The values of $1/n < 1$ delegate a favorable adsorption. Compared to the Freundlich isotherm, the higher correlation coefficient of Langmuir model confirmed the suitable of Langmuir model, indicating greater tendency of the homogeneous surface of K-nZVI.

3.4. Removal mechanism of Cr(VI) by K-nZVI

Characterizations analysis demonstrated that the removal process might include adsorption, reduction, and precipitation. Compared with the peak L and N in Fig. 3(b) and (d), they are so similar that peak N could be interpreted orally as the kaolin diffraction peak and nZVI had been partly consumed resulting in the disappearance of its diffraction peak. Though we cannot firmly conclude that iron oxides came into being due to the interferences of kaolin matrix diffraction peaks, it explicitly shows the characteristic peaks of compound $FeCr_2O_4$ referred to JCPDS (34-0,140) such as miller indices (1 1 1), (2 2 0), and (3 1 1) corresponding to two-theta 18.3˚ (magnified in the insert), 30.1˚, and 35.5˚, respectively. The conclusion of generation of co-precipitated $FeCr_2O_4$ is in good agreement with that of Shi et al. [11] and indicates that nZVI was oxidized to Fe^{2+} and simultaneously Cr(VI) was reduced to Cr(III), consequently facilitating the formation of co-precipitated $FeCr_2O_4$. The production of other chromium-iron deposits, of course, cannot be excluded.

In order to derive the removal mechanism better, XPS technique was used to analyze surface chemistry for K-nZVI particles extracted from 100 mg L^{-1} of Cr (VI) solution. Prior to each curve fitting, a Shirley-type background subtraction was preformed and no smoothing routine of raw data was done. All the spectra were curves fitted with Gaussian/Lorentzian functions to approximate the peak shapes. In order to eliminate the shifts caused by surface charging effects, the binding energy was referenced to the peak of aliphatic adventitious hydrocarbon C 1s band at 284.6 eV. The surface atomic concentration (at.%) was calculated by means of photoelectron peak areas and

Table 3
The relative contents of elements obtained from XPS spectra quantitative analysis

Peak	Position BE (eV)	FWHM (eV)	Raw area (cps eV)	ASF	Atomic conc. (at.%)
Fe 2p	710.900	4.509	35,747.0	2.957	2.19
Cr 2p	576.950	4.203	21,029.6	2.427	1.60
O 1s	531.750	1.982	273,409.4	0.780	65.45
C 1s	284.550	1.573	43,673.6	0.278	30.76

atomic sensitivity factors (ASF), for which the mathematical description is given by the equation:

$$\text{at.}\% = \frac{I_i/S_i}{\sum_j I_j/S_i} \times 100\% \quad (8)$$

where I and S denote the intensity of corresponding photoelectron peak (i.e. peak area) and ASF, respectively. The subscript i and j represent one certain element and total elements shown in Table 3, respectively.

The XPS spectra of K-nZVI after reaction (Fig. 11) reveal that chromium was incorporated into K-nZVI particles. In terms of the four elements (Fe, Cr, O, and C) (Fig. 11(a)), XPS spectra quantitative analysis provided information of surface composition and relevant parameters (Table 3). It is conductive to let us further

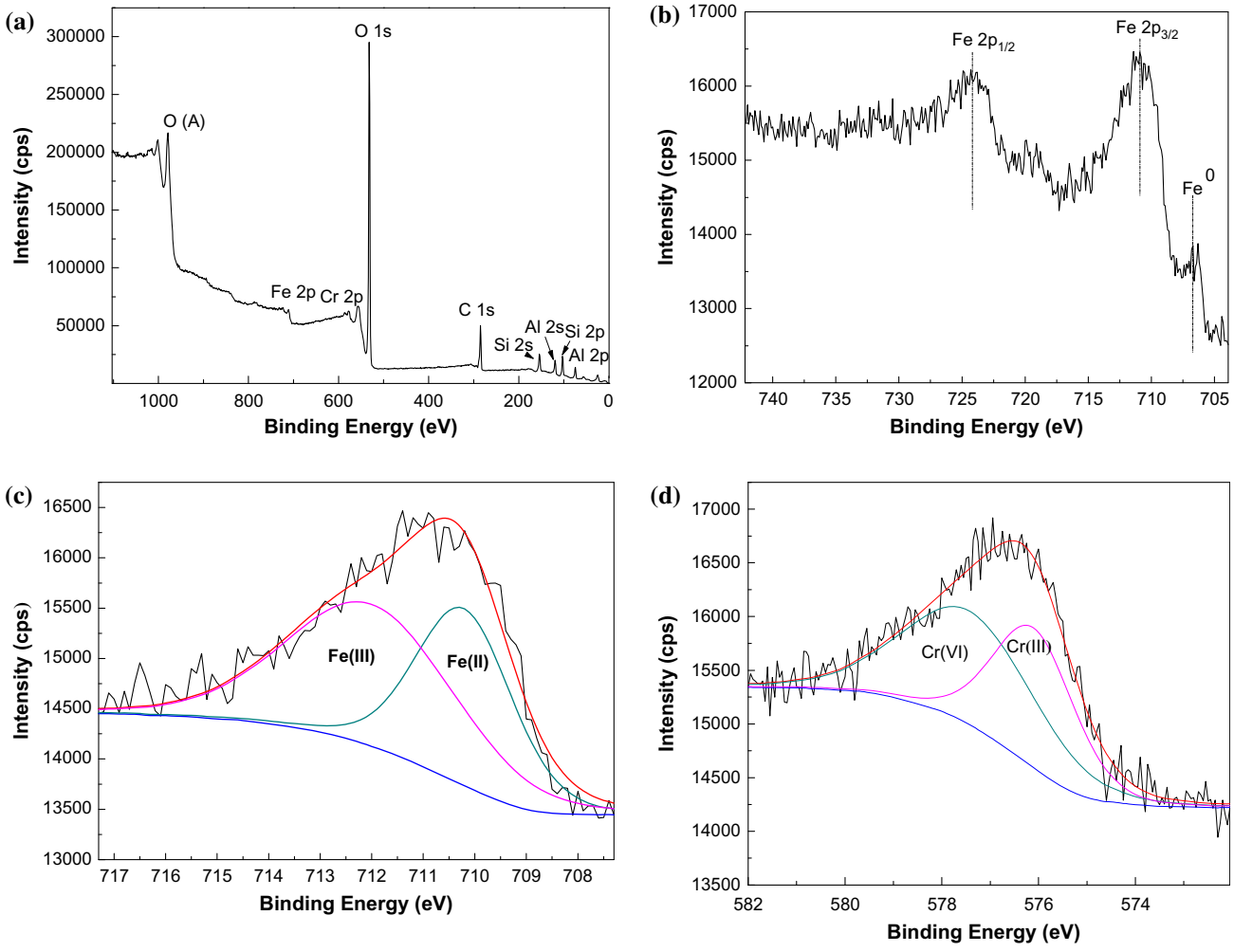

Fig. 11. XPS spectra for K-nZVI particles extracted from 100 mg L^{-1} Cr(VI) solution. (a) Full spectrum scanning, (b) Fe 2p, (c) curve fitting of Fe $2p_{3/2}$, and (d) curve fitting of Cr $2p_{3/2}$.

understand the whole reaction and draw some valuable conclusions. Firstly, considerable oxygen content could be construed as the contributions of iron (hydr) oxides, chromium (hydr)oxides, and the constituents of kaolin (e.g. SiO_2 and Al_2O_3) etc. Secondly, the atomic ratio of Fe and Cr is equal to ~1.4. However, due to the influences of iron (hydr)oxides and unreacted nZVI (see the following analysis), the actual atomic ratio for co-precipitation is uncertain.

For the high resolution scans of Fe 2p region (Fig. 11(b)), the first peak located at binding energy of 706.7 eV is Fe^0 $2p_{3/2}$. Peak position at 710.9 and 724.0 eV are assigned to Fe $2p_{3/2}$ and Fe $2p_{1/2}$, respectively [9]. Additionally, the shoulder peak at 719.9 eV belongs to the combination of shake-up satellite Fe $2p_{3/2}$ for oxidized iron and Fe $2p_{1/2}$ for Fe^0 [8]. Through curve fitting of Fe $2p_{3/2}$, it can be decomposed into two overlapping peaks at 710.2 eV and 712.0 eV, which correspond to Fe(II) and Fe(III), respectively [9]. The above results manifest that Fe^0 was superfluous and oxidized iron existed in mixed valence states after reaction (Fig. 11(c)). Thus, the oxidation of Fe^0 can be described by two successive elementary reactions:

$$Fe^0 = Fe^{2+} + 2e^- \quad (9)$$

$$Fe^{2+} = Fe^{3+} + e^- \quad (10)$$

A curve fitting of Cr $2p_{3/2}$ region (Fig. 11(d)) was also carried out and Cr $2p_{3/2}$ spectrum decomposed into two peaks representing Cr(III) and Cr(VI) located at 576.1 eV and 577.4 eV, respectively [9]. Using the area under each peak, a relative content of chromium in different valence was calculated: w[Cr(III)]:w[Cr(VI)] = 3,018.4/3,973.3 = 0.76. Therefore, during the remediation of Cr(VI), both redox and adsorption effects played important roles. In spite of redundant nZVI existed, adsorbed Cr(VI) still was unreduced suggesting that Fe^0 outer sphere was encompassed by passivation layers composed of Cr(III) and oxidized iron complexes.

The Cr(VI) removal by iron is surface mediated. Therefore, a close contact between Cr(VI) and iron surface is required. Kaolin can absorb a certain amount of chromium despite its low adsorption capacity. Consequently, the Cr(VI) concentration in the vicinity of iron surface increased. The adsorption facilitated the mass transfer of Cr(VI) from solution to iron surface, and then accelerated the removal of Cr(VI) in a synergetic way. The analogous synergetic effect has been found in some previous studies [37–39], in which enhanced removal of contaminants by nZVI was observed when the adsorbents had been combined.

Based on the results, the possible mechanism of Cr(VI) removal by K-nZVI in aqueous solution consists of four steps: (1) aqueous Cr(VI) ions are adsorbed on the surface of K-nZVI due to large specific surface area of K-nZVI (17.54 m^2 g^{-1}). The adsorption facilitated the mass transfer, and accelerated the reduction of Cr(VI) in a synergetic way; (2) the absorbed Cr(VI) is partly reduced to Cr(III) accompanied by Fe^0 oxidizing to Fe^{2+}; (3) oxidized Fe^{2+} continuously reacts with Cr(VI) and releases Fe^{3+} and Cr(III); and (4) on the outer surface of nZVI, Cr(III) and oxidized iron ions form passivation layers preventing the further removal of chromium and remaining adsorbed Cr(VI).

4. Conclusions

In this work, K-nZVI adsorbent was prepared by the liquid-phase chemical reduction method and used to remove chromate in aqueous solution. Comprehensive characterizations of kaolin, nZVI, and K-nZVI were carried out by SEM, FTIR, XRD, and XPS analyses, which illustrate that amorphous Fe^0 core/Fe_xO_y shell nZVI was successfully loaded into the pores and cracks and onto the surface of kaolin. The batch experiments illustrate that removal efficiency of Cr by K-nZVI decreased with increasing initial pH and Cr(VI) concentration, but increased while K-nZVI dosage increased. HA and phosphate had similar dual impacts on chromium removal by K-nZVI and the inhibitory effect was obvious at high concentration in spite of their different reaction mechanisms. In contract, high concentrations of sulfate and nitrate could advance chromium removal. To summarize, the positive effects of the three anions were ranked in: sulfate > nitrate > phosphate, while the negative impact of HA was notable. Adsorption isotherms indicate that the processes of chromate removal by K-nZVI were endothermic and the equilibrium adsorbed amount increased with elevating temperature. The Langmuir model correlated the adsorption isotherms was better than Freundlich model indicating greater tendency of homogeneous property of K-nZVI surface. At the conditions of 318 K and optimized pH 4.0, the maximum adsorption capacity was 33.39 mg g^{-1} illustrating that K-nZVI was effective for the removal of total Cr. Adsorption, redox reaction, and precipitation are all involved during the process of chromate removal by K-nZVI. The potential removal mechanism of chromate by K-nZVI is suggested based on our results. However, it should be noted that natural environment has much complicated components and variable pH, the functioning

of K-nZVI in combination of co-existing ions and at realistic pH should be further studied.

Acknowledgment

This research was supported by the Key Basic Research Program of the Sichuan Provincial Education Commission, China (Grant No. 09ZA062).

References

[1] C.D. Palmer, P.R. Wittbrodt, Processes affecting the remediation of chromium-contaminated sites, Environ. Health Perspect. 92 (1991) 25.
[2] A. Lu, S. Zhong, J. Chen, J. Shi, J. Tang, X. Lu, Removal of Cr(VI) and Cr(III) from aqueous solutions and industrial wastewaters by natural clino-pyrrhotite, Environ. Sci. Technol. 40 (2006) 3064–3069.
[3] M.D. Cohen, B. Kargacin, C.B. Klein, M. Costa, Mechanisms of chromium carcinogenicity and toxicity, Crit. Rev. Toxicol. 23 (1993) 255–281.
[4] F.L. Fu, W.J. Han, C.J. Huang, B. Tang, M. Hu, Removal of Cr(VI) from wastewater by supported nanoscale zero-valent iron on granular activated carbon, Desalin. Water Treat. 51 (2013) 2680–2686.
[5] Z.Q. Fang, X.Q. Qiu, R.X. Huang, X.H. Qiu, M.Y. Li, Removal of chromium in electroplating wastewater by nanoscale zero-valent metal with synergistic effect of reduction and immobilization, Desalination 280 (2011) 224–231.
[6] T.S. Anirudhan, P.G. Radhakrishnan, Chromium(III) removal from water and wastewater using a carboxylate-functionalized cation exchanger prepared from a lignocellulosic residue, J. Colloid Interface Sci. 316 (2007) 268–276.
[7] X.H. Guan, H.R. Dong, J. Ma, Influence of phosphate, humic acid and silicate on the transformation of chromate by Fe(II) under suboxic conditions, Sep. Purif. Technol. 78 (2011) 253–260.
[8] X.Q. Li, J.S. Cao, W.X. Zhang, Stoichiometry of Cr(VI) immobilization using nanoscale zerovalent iron (nZVI): A study with high-resolution X-ray photoelectron spectroscopy (HR-XPS), Ind. Eng. Chem. Res. 47 (2008) 2131–2139.
[9] X.S. Lv, J. Xu, G.M. Jiang, J. Tang, X.H. Xu, Highly active nanoscale zero-valent iron (nZVI)-Fe_3O_4 nanocomposites for the removal of chromium(VI) from aqueous solutions, J. Colloid Interface Sci. 369 (2012) 460–469.
[10] W.X. Zhang, Nanoscale iron particles for environmental remediation: An overview, J. Nanopart. Res. 5 (2003) 323–332.
[11] L.N. Shi, Y.M. Lin, X. Zhang, Z.L. Chen, Synthesis, characterization and kinetics of bentonite supported nZVI for the removal of Cr(VI) from aqueous solution, Chem. Eng. J. 171 (2011) 612–617.
[12] S.M. Ponder, J.G. Darab, T.E. Mallouk, Remediation of Cr(VI) and Pb(II) aqueous solutions using supported, nanoscale zero-valent iron, Environ. Sci. Technol. 34 (2000) 2564–2569.
[13] B. Geng, Z.H. Jin, T.L. Li, X.H. Qi, Preparation of chitosan-stabilized Fe^0 nanoparticles for removal of hexavalent chromium in water, Sci. Total Environ. 407 (2009) 4994–5000.
[14] Y.M. Li, J.F. Li, Y.L. Zhang, Mechanism insights into enhanced Cr(VI) removal using nanoscale zerovalent iron supported on the pillared bentonite by macroscopic and spectroscopic studies, J. Hazard. Mater. 227 (2012) 211–218.
[15] L.B. Hoch, E.J. Mack, B.W. Hydutsky, J.M. Hershman, J.M. Skluzacek, T.E. Mallouk, Carbothermal synthesis of carbon-supported nanoscale zero-valent iron particles for the remediation of hexavalent chromium, Environ. Sci. Technol. 42 (2008) 2600–2605.
[16] P. Yuan, M. Fan, D. Yang, H. He, D. Liu, A. Yuan, J. Zhu, T. Chen, Montmorillonite-supported magnetite nanoparticles for the removal of hexavalent chromium [Cr(VI)] from aqueous solutions, J. Hazard. Mater. 166 (2009) 821–829.
[17] S.Z. Li, P.X. Wu, H.L. Li, N.W. Zhu, P. Li, J.H. Wu, X.D. Wang, Z. Dang, Synthesis and characterization of organo-montmorillonite supported iron nanoparticles, Appl. Clay Sci. 50 (2010) 330–336.
[18] X. Zhang, S. Lin, X.Q. Lu, Z.L. Chen, Removal of Pb (II) from water using synthesized kaolin supported nanoscale zero-valent iron, Chem. Eng. J. 163 (2010) 243–248.
[19] Ç. Üzüm, T. Shahwan, A. Eroğlu, K. Hallam, T. Scott, I. Lieberwirth, Synthesis and characterization of kaolinite-supported zero-valent iron nanoparticles and their application for the removal of aqueous Cu^{2+} and Co^{2+} ions, Appl. Clay Sci. 43 (2009) 172–181.
[20] Z.X. Chen, T. Wang, X.Y. Jin, Z.L. Chen, M. Megharaj, R. Naidu, Multifunctional kaolinite-supported nanoscale zero-valent iron used for the adsorption and degradation of crystal violet in aqueous solution, J. Colloid Interface Sci. 398 (2013) 59–66.
[21] X. Zhang, S. Lin, Z. Chen, M. Megharaj, R. Naidu, Kaolinite-supported nanoscale zero-valent iron for removal of Pb^{2+} from aqueous solution: Reactivity, characterization and mechanism, Water Res. 45 (2011) 3481–3488.
[22] P.C. Ryan, F.J. Huertas, The temporal evolution of pedogenic Fe-smectite to Fe-kaolin via interstratified kaolin–smectite in a moist tropical soil chronosequence, Geoderma 151 (2009) 1–15.
[23] Z.X. Chen, Y. Cheng, Z.L. Chen, M. Megharaj, R. Naidu, Kaolin-supported nanoscale zero-valent iron for removing cationic dye–crystal violet in aqueous solution, J. Nanopart. Res. 14 (2012) 1–8.
[24] Y.P. Sun, X.Q. Li, J. Cao, W.X. Zhang, H.P. Wang, Characterization of zero-valent iron nanoparticles, Adv. Colloid Interface Sci. 120 (2006) 47–56.
[25] P.D. Saha, A. Dey, P. Marik, Batch removal of chromium (VI) from aqueous solutions using wheat shell as adsorbent: Process optimization using response surface methodology, Desalin. Water Treat. 39 (2012) 95–102.
[26] W.F. Liu, J. Zhang, C.L. Zhang, L. Ren, Preparation and evaluation of activated carbon-based iron-containing adsorbents for enhanced Cr(VI) removal: Mechanism study, Chem. Eng. J. 189–190 (2012) 295–302.
[27] Y. Xie, D.M. Cwiertny, Influence of anionic cosolutes and pH on nanoscale zerovalent iron longevity: Time scales and mechanisms of reactivity loss toward 1,1,1,2-tetrachloroethane and Cr(VI), Environ. Sci. Technol. 46 (2012) 8365–8373.

[28] B. Geng, Z.H. Jin, T.L. Li, X.H. Qi, Kinetics of hexavalent chromium removal from water by chitosan-Fe^0 nanoparticles, Chemosphere 75 (2009) 825–830.
[29] T.Z. Liu, P.H. Rao, I.M.C. Lo, Influences of humic acid, bicarbonate and calcium on Cr(VI) reductive removal by zero-valent iron, Sci. Total Environ. 407 (2009) 3407–3414.
[30] Q. Wang, N. Cissoko, M. Zhou, X. Xu, Effects and mechanism of humic acid on chromium (VI) removal by zero-valent iron (Fe^0) nanoparticles, Phys. Chem. Earth. 36 (2011) 442–446.
[31] L.E. Eary, D. Rai, Chromate removal from aqueous wastes by reduction with ferrous ion, Environ. Sci. Technol. 22 (1988) 972–977.
[32] C.L. Tang, Z.Q. Zhang, X.N. Sun, Effect of common ions on nitrate removal by zero-valent iron from alkaline soil, J. Hazard. Mater. 231–232 (2012) 114–119.
[33] J. Gui, T. Devine, The influence of sulfate ions on the surface enhanced Raman spectra of passive films formed on iron, Corros. Sci. 36 (1994) 441–462.
[34] L. Xie, C. Shang, The effects of operational parameters and common anions on the reactivity of zero-valent iron in bromate reduction, Chemosphere 66 (2007) 1652–1659.
[35] C.P. Huang, H.W. Wang, P.C. Chiu, Nitrate reduction by metallic iron, Water Res. 32 (1998) 2257–2264.
[36] Y.C. Sharma, V. Srivastava, C.H. Weng, S.N. Upadhyay, Removal of Cr(VI) from wastewater by adsorption on iron nanoparticles, Can. J. Chem. Eng. 87 (2009) 921–929.
[37] Y.M. Li, Y. Zhang, J.F. Li, X.M. Zheng, Enhanced removal of pentachlorophenol by a novel composite: Nanoscale zero valent iron immobilized on organo-bentonite, Environ. Pollut. 159 (2011) 3744–3749.
[38] Y. Zhang, Y.M. Li, J.F. Li, L.J. Hu, X.M. Zheng, Enhanced removal of nitrate by a novel composite: Nanoscale zero valent iron supported on pillared clay, Chem. Eng. J. 171 (2011) 526–531.
[39] G.D. Sheng, X.Y. Shao, Y.M. Li, J.F. Li, H.P. Dong, W. Cheng, X. Gao, Y.Y. Huang, Enhanced removal of uranium(VI) by nanoscale zerovalent iron supported on Na–Bentonite and an investigation of mechanism, J. Phys. Chem. A 118 (2014) 2952–2958.